Biosensors and Bioelectronics 99 (2018) 223–229

Contents lists available at ScienceDirect

Biosensors and Bioelectronics

journal homepage: www.elsevier.com/locate/bios

A highly stable acetylcholinesterase biosensor based on chitosan-TiO_2-graphene nanocomposites for detection of organophosphate pesticides

Hui-Fang Cui*, Wen-Wen Wu, Meng-Meng Li, Xiaojie Song, Yuanxu Lv, Ting-Ting Zhang

Department of Bioengineering, School of Life Sciences, Zhengzhou University, 100 Science Avenue, Zhengzhou 450001, PR China

ARTICLE INFO

Keywords:
Acetylcholinesterase
Organophosphorus pesticides
Dichlorvos
Biosensor
TiO_2 sol-gel
Chitosan

ABSTRACT

A highly stable electrochemical acetylcholinesterase (AChE) biosensor for detection of organophosphorus pesticides (OPs) was developed simply by adsorption of AChE on chitosan (CS), TiO_2 sol-gel, and reduced graphene oxide (rGO) based multi-layered immobilization matrix (denoted as CS@TiO_2-CS/rGO). The biosensor fabrication conditions were optimized, and the fabrication process was probed and confirmed by scanning electron microscopy and electrochemical techniques. The matrix has a mesoporous nanostructure. Incorporation of CS and electrodeposition of a CS layer into/on the TiO_2 sol-gel makes the gel become mechanically strong. The catalytic activity of the AChE immobilized CS@TiO_2-CS/rGO/glassy carbon electrode to acetylthiocholine is significantly higher than those missing any one of the component in the matrix. The detection linear range of the biosensor to dichlorvos, a model OP compound, is from 0.036 μM (7.9 ppb) to 22.6 μM, with a limit of detection of 29 nM (6.4 ppb) and a total detection time of about 25 min. The biosensor is very reproducibly and stable both in detection and in storage, and can accurately detect the dichlorvos levels in cabbage juice samples, providing an efficient platform for immobilization of AChE, and a promisingly applicable OPs biosensor with high reliability, simplicity, and rapidness.

1. Introduction

Pesticides, especially organophosphorus pesticides (OPs) have been widely used in the past several decades to protect crops from insects. However, OP pesticides are toxic to human and most animals through inhibition of the enzymes in neurosynapses—acetylcholinesterases (AChE), resulting in accumulation of acetylcholine in human body, over stimulating its receptors in synapses and eventually damaging the nervous system (Patocka et al., 2004; Long et al., 2015; Costa, 2006; Eddleston et al., 2008; Fukuto, 1990). Detection of OPs in various samples with high reliability, simplicity, and rapidness has become increasingly necessary.

In the past decades, great efforts have been made to develop efficient and simple methods to determine OPs levels (Long et al., 2015; Lu and Xia, 2015; Qian and Lin, 2015; Yu et al., 2015). Among them, electrochemical methods have many advantages such as high reliability, simple instruments, fast result acquirement, easiness for operation, high sensitivity, and compatible to complex samples. The detection mechanism usually depends on the AChE catalyzed reaction of acetylthiocholine (ATCl) to produce the electro-active thiocholine (TCl) (Wei and Wang, 2015; Yu et al., 2015). Inhibition of the AChE activity by OPs would result in reduced TCl production of the biosensor. In development of practically applicable electrochemical biosensors, effective immobilization of AChE while maintaining its native catalytic activity is one of the key considerations; the electrocatalytic activity of the electrode to TCl, and the transport of the enzymatic reaction related molecules through the biofilm are also the main factors; the stability of the biosensor is the last key factor. Recently, the advances in nanotechnology have provided various nanomaterials with special properties, such as high specific surface area and high electrocatalytic activity, for fabrication of AChE electrochemical biosensors (Shi et al., 2006; Sundarmurugasan et al., 2016; Wei and Wang, 2015; Yu et al., 2015). However, most of the reported AChE electrochemical biosensors still face serious instability problems.

TiO_2 porous sol-gel film as a protein immobilization matrix has attracted great attention due to its large specific surface area, low cost, non-toxicity, good thermal and chemical stability, semi-conductivity, and excellent biocompatibility (Cui et al., 2013; Yu and Ju, 2002; Zhu et al., 2009). However, the TiO_2 gel, when fabricated on smooth solid surfaces as a monolithic part, suffers from the drawbacks of low adhesion and high fragility, resulting in the loss of sensor stability upon immersion in water. Blending polymer with nanomaterials to form nanocomposites has been an effective strategy to reinforcing the mechanical strength of each component (Behera et al., 2017; Tang

* Corresponding author.
E-mail address: hfcui@zzu.edu.cn (H.-F. Cui).

http://dx.doi.org/10.1016/j.bios.2017.07.068
Received 31 May 2017; Received in revised form 24 July 2017; Accepted 28 July 2017
Available online 29 July 2017

et al., 2016; Yang et al., 2017).

Graphene as a carbon nanomaterial has attracted tremendous research interests in various applications due to its large surface area, excellent thermal/chemical stability, high electronic/thermal conductivity, and superior mechanical flexibility (Bai et al., 2014; Balandin et al., 2008; Feng et al., 2013; Ge et al., 2017a, 2017b; Geim, 2009; Novoselov et al., 2004; Tang et al., 2011), and has contributed greatly as a component of AChE immobilization matrices in electrochemical biosensor fabrication, mainly by improving the matrix electro-conductivity and surface area (Chen et al., 2016; Li et al., 2017; Wang et al., 2016).

In this study, by taking dichlorvos (DDVP) as a model OP, we investigated the usage of TiO_2 sol-gel film as an immobilization matrix, and chitosan (CS), a well-known biocompatible and positively charged polymer as an incorporation polymer in the TiO_2 sol-gel, for AChE biosensor fabrication on glassy carbon (GC) electrode. To further improve the matrix mechanical stability and the immobilization efficiency for the negatively charged AChE, a CS layer was electrodeposited onto the TiO_2-CS blending gel, resulting in a multi-layered matrix (denoted as CS@TiO_2-CS). Reduced graphene oxide (rGO) was introduced as an rGO film onto the GC electrode to improve the sensor sensitivity. The AChE biosensor fabrication procedure was characterized and optimized, and the performance of the biosensor in DDVP detection was evaluated. Finally, the sensitive, simple, and highly stable AChE biosensor was evaluated for applications in DDVP detection in vegetable samples.

2. Experimental

2.1. Materials and chemicals

AChE (from electric eel) and ATCl were from Sigma-Aldrich. CS (viscosity > 400 mPa s) and DDVP (1 mg mL^{-1} in methanol) were from Aladdin Bio-Chem Technology (Shanghai, China). Graphene oxide (GO) (thickness: 0.8~1.2 nm, lateral size: 1~5 μm, purity: > 99%) was from Nanjing XFNANO Materials Tech. (China). Other remaining chemicals were obtained from Sinopharm Chemical Reagent (Shanghai, China). All chemicals were of analytical grade and used as received. Purified nitrogen with a purity of 99.99% was obtained from Zhengzhou Keyi Industrial Gas (China). Deionized water obtained from a Millipore water system was used throughout the experiment.

2.2. Apparatus and measurement

The modified GC electrode was probed by scanning electron microscopy (SEM, JEOL JSM-7500F), and also characterized by cyclic voltammetry (CV) and electrochemical impedance spectroscopy (EIS) techniques. Fourier transform infrared (FTIR) spectra were collected using PerkinElmer Spectrum 2 FTIR spectrophotometer. The CVs were performed in 0.01 M phosphate buffer (PBS, pH 7.4), or in 5 mM $K_3[Fe(CN)_6]$ supported by 1 M KCl. The EIS measurement was performed in 0.1 M KCl containing equimolar $[Fe(CN)_6]^{3-/4-}$ (10/10 mM) with AC frequency from 0.1 Hz to 100 kHz. The effective surface area (A, cm^2) of the electrodes was obtained by running CVs at various scan rates in the 5 mM $K_3[Fe(CN)_6]$ (detailed in Supplementary Material). All electrochemical measurements were performed at room temperature (~25 °C) using a CHI-660E electrochemical workstation (Shanghai Chenhua Instrument, China) in a three-electrode arrangement consisting of a working electrode (modified GC electrode), a Pt counter electrode and an Ag|AgCl|KCl (3 M) reference electrode.

2.3. Preparation of rGO

The rGO as a black suspension (0.3 mg mL^{-1}) was prepared from GO as described by Park and Ruoff (2009), in our previous paper (Bai et al., 2014), and also in the Supplementary Material.

2.4. Preparation of TiO_2 sol-gel, CS solution and TiO_2-CS sol-gel

The TiO_2 and the TiO_2-CS sol-gel can be formed in minutes from the respective precursor solution upon exposure a thin layer of the solution to air. The TiO_2 precursor solution was synthesized as described in the Supplementary Material. The TiO_2-CS precursor solutions were prepared by mixing the TiO_2 precursor solution with a CS solution of various concentrations, at different volume ratios. The CS solutions were prepared by dissolving 1 g CS in 100 mL 1% (vol%) acetic acid solution, and then diluting the 1% CS solution to various concentrations with water.

2.5. Fabrication of the biosensor

The GC electrode was cleaned by being polished consecutively with 0.3 and 0.05 μm alumina powder, followed by sonication in water bath. The as-prepared rGO suspension was diluted to 0.2 mg mL^{-1} with ethanol, and 4 μL of the diluted rGO was cast on the dried GC electrode. After air-dried, the rGO/GC electrode was coated with 4 μL of TiO_2-CS solution, and then left in the air for gelation. The volume content of the TiO_2 sol-gel, and the weight content of CS in the TiO_2-CS mixture was varied from 90.0% to 99.5% (taken the as-synthesized TiO_2 gel as 100%), and from 0.002% to 0.020%, respectively, to obtain an optimum biosensor. The resulted TiO_2-CS composites are denoted as $TiO_2^{90.0}$-$CS^{0.002}$ etc., accordingly. For simplification, the optimized TiO_2-CS nanocomposite, $TiO_2^{99.0}$-$CS^{0.005}$ (shown in Section 3.3), is also named as TiO_2^{m}-CS^{m}. Afterwards, a CS layer was electrodeposited on the TiO_2-CS/rGO/GC surface by holding the potential at −2.5 V for seconds in 0.2% CS. Finally, AChE was immobilized on the $CS^{@}TiO_2$-CS/rGO/GC electrode by dropping 4 μL AChE solution (in PBS, containing 1% bovine serum albumin) onto the electrode surface. The as-fabricated enzyme electrode was dried in the air and kept at 4 °C, ready for used.

2.6. Electrocatalytic and sensing performance

The electrocatalytic performance to ATCl was investigated by differential pulse voltammetry (DPV) technique (from 0.2 to 1.0 V; amplitude, 0.05 V; pulse width, 0.005 s; pulse period, 0.02 s) in PBS. Before the DPV measurement, the electrode was cleaned by running CVs in PBS until a stable CV curve was obtained, to remove loosely adsorbed AChE. The sensing performance to DDVP was evaluated by recording DPVs in PBS containing 1 mM ATCl before and after incubating the electrode in a DDVP solution for 10 min. The inhibition ratio (Inhibit%) of DDVP to the enzyme electrode, which was taken as the sensing signal towards OPs, was determined from Eq. (1), where I_{cat}^{0} and $I_{cat}^{'}$ represents the DPV peak current in response to 1 mM ATCl before and after, respectively, the DDVP incubation.

$$\text{Inhibit\%} = (1 - I_{cat}'/I_{cat}^{0}) \times 100\% \quad (1)$$

The detection stability was evaluated by repetitively recording the DPVs in 1 mM ATCl. The storage stability was evaluated by monitoring the DPVs in 1 mM ATCl during a wet storage in sterilized PBS at 4 °C, and a dry storage at −20 °C, respectively, for 30 days. The electrodes were taken out for the ATCl test every 10 days during the storage period.

2.7. Detection of vegetable samples

The applicability of the biosensor was evaluated by detecting DDVP levels in DDVP spiked cabbage juice samples. For preparation of the juice samples, cabbage was firstly cleaned with water and then dried in the air. Then 100 g cabbage pieces were mixed with 100 mL PBS (0.02 M, pH 7.4) in a homogenizer at room temperature. The cabbage homogenate was then centrifuged at 5000 rpm for 10 min, and the

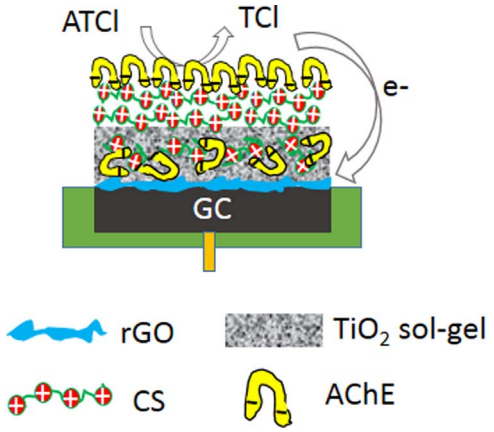

Scheme 1. Schematic illustration of the AChE biosensor structure and its working mechanism to ATCl.

supernatant was taken as the cabbage juice samples. The biosensor was incubated with the cabbage juice samples, which were spiked in advance with DDVP, for 10 min, and then subject to DPV detection in 1 mM ATCl. The Inhibit% values were compared with the calibration curve to obtain the found OPs concentration.

3. Results and discussion

3.1. Characterization of the fabrication process

The structure of the as-fabricated biosensor was schematically shown in Scheme 1. The surface morphology of the electrode after each fabrication process was probed by SEM (Fig. 1). The rGO nanosheets (Fig. 1A) have a crumpled surface morphology, a typical feature of graphene. The TiO_2 sol-gel film (Fig. 1B) shows a homogeneous mesoporous morphology composed of interconnected nanoparticles of ~6.5 nm, and pores of ~6.3 nm in diameter. With the incorporation of CS (Fig. 1C and D), the surface become rougher and the nanoparticles get bigger. The content of TiO_2 has no very obvious effect on the surface morphology. The electrodeposited CS layer coalesces the TiO_2-CS composite nanoparticles, forming nanoparticle aggregates, but the surface is still rough and porous (Fig. 1E). AChE loading fills the pores, resulting in a much smoother surface (Fig. 1F). The rough and porous surface morphology would facilitate an effective AChE loading.

The fabrication process was also characterized by electrochemical techniques. The cyclic voltammograms (CVs) of the GC electrode without and with modifications in the neutral PBS are illustrated in Fig. S-1 (Supplementary Material). The intensity of the double layer current could positively reflect the electrode surface area. The rGO film obviously increased the double layer current. As a highly conductive and high specific surface area nanomaterial, the graphene film appreciably increases the electrode surface area as expected.

The electrochemical properties of the modified electrodes were probed with $K_3[Fe(CN)_6]$ (Fig. 2A). At all the electrodes, a symmetric pair of peaks with E_0' of about +0.26 V from the redox reactions of $[Fe(CN)_6]^{3-}$ were observed. The casted rGO film obviously increased the redox peak current (Ip), with the effective surface area (A) increased from 0.052 to 0.068 cm^2 (Fig. S-3 in Supplementary Material), without obvious affection to the peak potential separations (~63 mV) (curve b). The crumpled surface morphology and the multilayer structure of the rGO nanosheets should contribute to the increased 'A' value. Introduction of the TiO_2-CS nanocomposites dramatically decreased the redox currents (curve c), owing to the semi-conductivity of TiO_2, the non-conductivity of CS, and the negatively charged surface of the TiO_2 gel. In contrast, the electrodeposition of the CS film on TiO_2-CS obviously increased the redox currents (curve d). Although CS is non-conductive, the positive charges of the CS film would adsorb and accumulate the negative-charged $K_3[Fe(CN)_6]$ probe molecules. The decreased redox currents with the AChE casting (curve e) indicate the successful immobilization of AChE, which is non-conductive and negatively charged in neutral conditions.

EIS technique, which can provide the information of membrane capacitance and resistance (Gao et al., 2001), was then used to probe

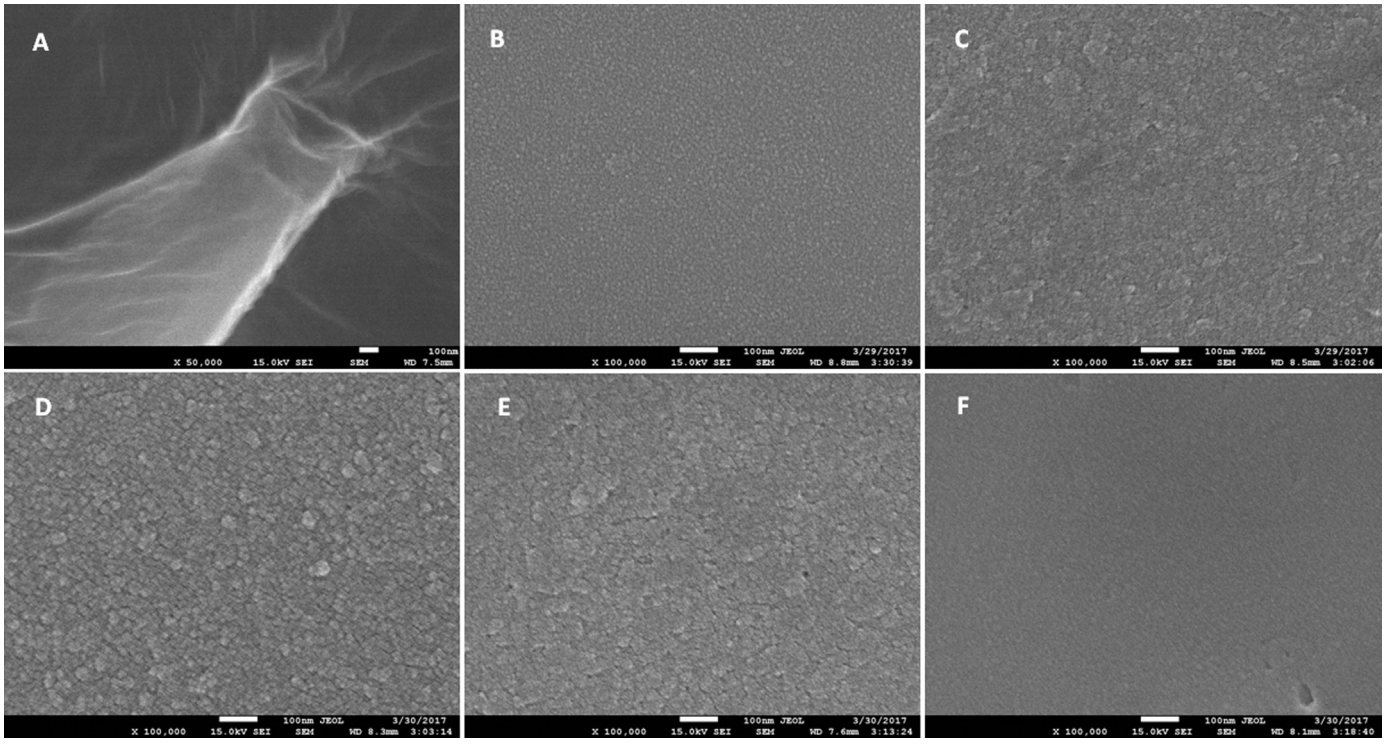

Fig. 1. SEM images of (A) rGO/GC, (B) TiO_2/rGO/GC, (C) $TiO_2^{99.0}$-$CS^{0.005}$/rGO/GC (i.e. TiO_2^{m}-CS^{m}/rGO/GC), (D) $TiO_2^{90.0}$-$CS^{0.005}$/rGO/GC, (E) $CS^{@}TiO_2^{m}$-CS^{m}/rGO/GC, and (F) AChE/$CS^{@}TiO_2^{m}$-CS^{m}/rGO/GC electrodes. The electrodeposition time for CS layer: 15 s, AChE concentration: 5 mg mL^{-1}.

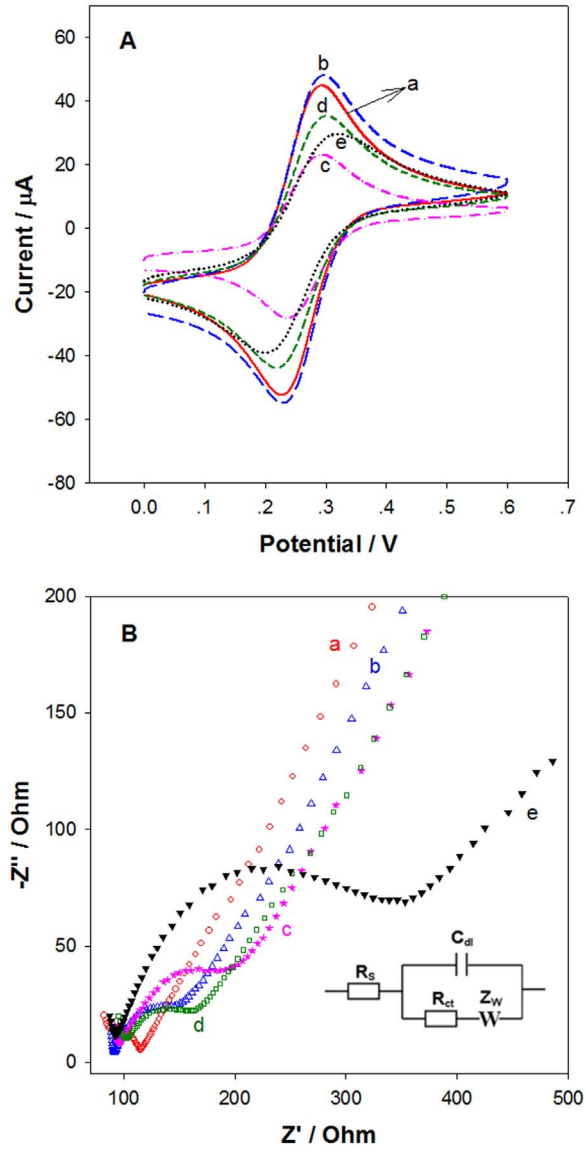

Fig. 2. (A) The CVs, and (B) the EIS of (a) GC, (b) rGO/GC, (c) TiO_2^m-CS^m/rGO/GC, (d) $CS^{@}TiO_2^m$-CS^m/rGO/GC, and (e) AChE/$CS^{@}TiO_2^m$-CS^m/rGO/GC electrodes, in (A) 5 mM $K_3[Fe(CN)_6]$, scan rates: 0.05 V s^{-1}, and (C) $[Fe(CN)_6]^{3-/4-}$ (10/10 mM). The electrodeposition time for CS layer: 20 s, AChE concentration: 5 mg mL^{-1}.

the biosensor fabrication process. The Nyquist complex plane plots of all the electrodes exhibit a single semicircle at high frequency domain and a straight line at low frequency domain (Fig. 2B). The linear tail with a slope of unity is dominated by the interfacial mass transfer of the redox species, while the semicircle impedance is mainly contributed by the charge-transfer resistance (R_{ct}) and the double-layer capacitance (C_{dl}) of the electrode surface. The R_{ct} value of the rGO/GC electrode, which can be determined by ZSimpWin (Princeton Applied Research) using a modified Randles circuit (Inset in Fig. 2C), was about 43 Ω, slightly larger than that of the GC electrode (~ 23 Ω). The large surface area and the inter-sheets barrier of the rGO film should contribute to the increased charge-transfer resistance. With the introduction of the TiO_2-CS nanocomposites, CS film, and AChE, the R_{ct} value increased to ~ 94 Ω, then decreased to ~ 59 Ω, and finally dramatically increased to ~ 279 Ω, respectively, consistent with the CV experimental results in $K_3[Fe(CN)_6]$. It should be noted that introduction of the CS film drastically decreased the R_{ct} value, owing to the adsorption and accumulation of the negative-charged probe molecules to the positively charged CS film. The CS layer should also be able to enhance the adsorption amount and stability of the negatively charged AChE in the biosensor fabrication.

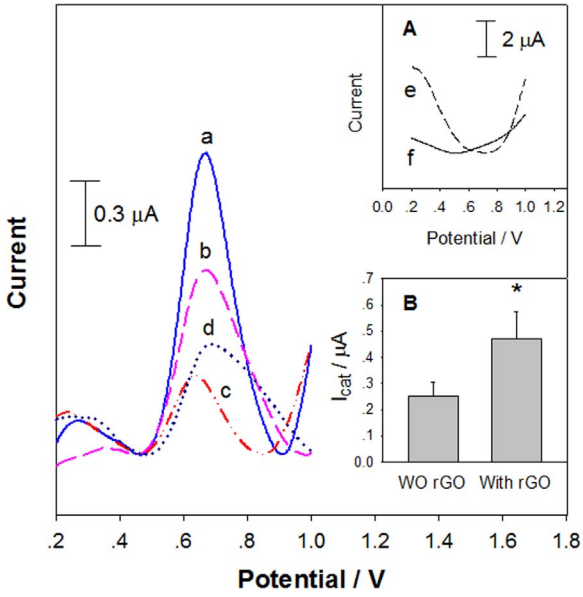

Fig. 3. The DPVs of (a) AChE/$CS^{@}TiO_2^m$-CS^m/rGO/GC, (b) AChE/$CS^{@}TiO_2^m$-CS^m/GC, (c) AChE/TiO_2^m-CS^m/rGO/GC, and (d) AChE/$CS^{@}TiO_2$/rGO/GC in PBS containing 1 mM ATCl. (Inset A) The DPVs of (e) AChE/CS/rGO/GC in PBS containing 1 mM ATCl, and (f) AChE/$CS^{@}TiO_2^m$-CS^m/rGO/GC in blank PBS. (Inset B) The statistic I_{cat} values of the AChE/$CS^{@}TiO_2^m$-CS^m/rGO/GC (with rGO), and AChE/$CS^{@}TiO_2^m$-CS^m/GC (WO rGO) electrodes in 1 mM ATCl. The electrodeposition time for CS layer: 20 s, AChE concentration: 5 mg mL^{-1}. For the curve a, b, c, and d, the baseline was corrected. ** represents that the p value is less than 0.01 in the *t*-test (n = 3–5).

3.2. Component effect of the biosensor

The DPV curves of the biosensor with various components of immobilization matrix in 1 mM ATCl are shown in Fig. 3. For the AChE/$CS^{@}TiO_2$-CS/rGO/GC electrode (curve a), a very strong oxidation peak (peak current, I_{cat}, ~ 1.46 μA) appeared in the ATCl solution at the potential of ~ 0.65 V, indicating that the immobilized AChE is bioactive, and the enzymatic product TCl can be electro-oxidized efficiently at the electrode (Scheme 1). The DPV peak current increased with the incubation time in ATCl solution, and reached plateau at 6 ~ 9 min (Fig. S-4 in Supplementary Material), depending on the diffusion rate of ATCl and TCl in the immobilization matrix and the enzymatic reaction rate. The incubation time with maximum peak currents was chosen and employed for the biosensing application in this study. The DDVP detection time with the biosensor, including the incubation time in ATCl solution, and the incubation time in DDVP samples, was therefore about 25 min in total. When rGO was absent in the biosensor composition (curve b, and Inset B in Fig. 3), the exhibited I_{cat} value (~ 0.70 μA) was significantly smaller, suggesting that rGO can catalyze the electro-oxidation of TCl. Graphene has shown high electro-catalytic activity to many molecules, such as dopamine (Bai et al., 2014). For the biosensors without the CS layer (curve c) (I_{cat}: ~ 0.37 μA), and those without incorporation of CS into the TiO_2 sol-gel (curve d) (I_{cat}: ~ 0.51 μA), in addition to a lower I_{cat} value, the detection signals for ATCl were not very reproducible due to mechanical instability of the immobilization matrices. Both the electrodeposited CS layer, and the incorporated CS in the TiO_2-CS nanocomposites could greatly improve the mechanical stability of the immobilization matrix, as also observed by our naked eyes. In addition, the positively charged CS layer may not only enhance the AChE adsorption amount and stability, and also facilitate a favorable AChE orientation and conformation (as shown in Scheme 1). The net surface of AChE with an isoelectric point of 5.5 is negatively charged in neutral conditions (Choi et al., 2001), and the active-site gorge region of AChE was also investigated to be negatively

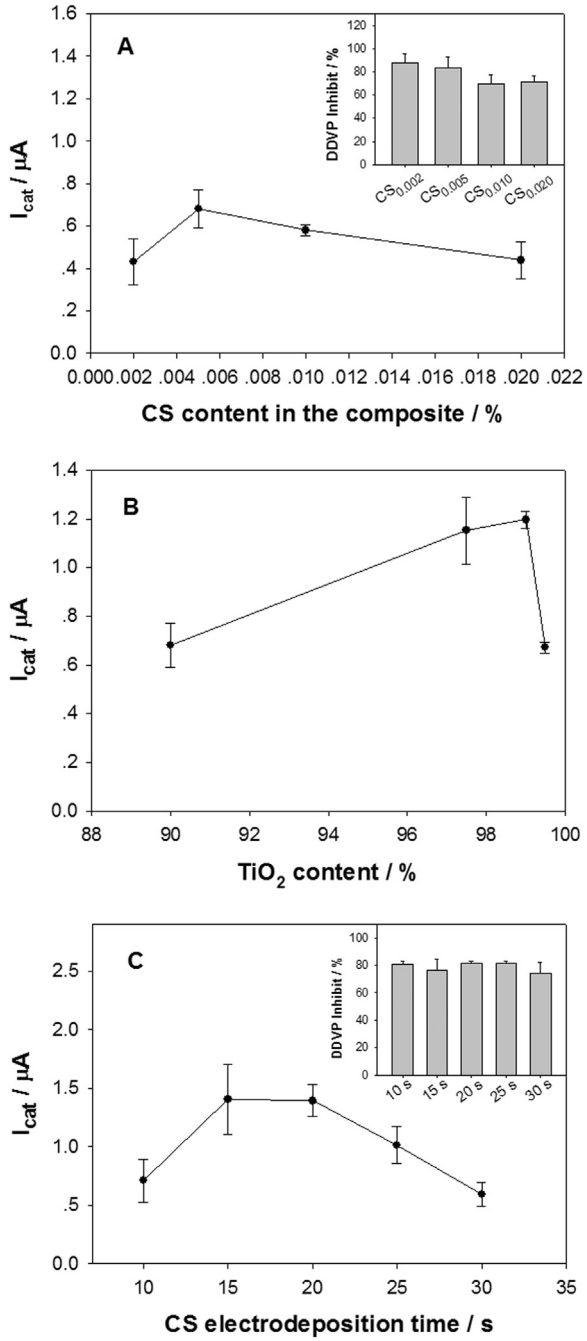

Fig. 4. The I_{cat} values of (A) AChE/$CS^{@}TiO_2^{90.0}$-CS/rGO/GC, (B) AChE/$CS^{@}TiO_2$-$CS^{0.005}$/rGO/GC, and (C) AChE$^{@}$CS/TiO_2^{m}-CS^{m}/rGO/GC electrodes in 1 mM ATCl. The electrodeposition time for the CS layer in (A, B) was 15 s. The AChE concentration for the enzyme loading in (A, B) was 5 mg mL^{-1}, and (C) was 25 mg mL^{-1}. (Insets in A and C) The Inhibit% of 22.6 μM DDVP to the ATCl response, n = 3–5.

charged (Dvir et al., 2010; Ripoll et al., 1993), resulting in the efficient immobilization of AChE onto the $CS^{@}TiO_2$-CS matrix mainly through electrostatic interaction. In contrast, the incorporation of CS into the TiO_2 sol-gel should also be able to enhance the AChE immobilization amount, due to the rougher structure as probed by SEM. It should be especially noted that the electrode without the TiO_2 or the TiO_2-CS gel (curve e in Inset A) did not show any obvious oxidation peak in the potential range, indicating that AChE was not efficiently immobilized. The mesoporous nanostructure of the TiO_2 sol-gel, in addition to its large specific surface area, non-toxicity, semi-conductivity, and excellent biocompatibility, facilitates an effective AChE loading, exhibits a high electrocatalytic activity to TCl, and provides an excellent microenvironment for AChE.

3.3. Optimization of the biosensor

The fabrication conditions were optimized. Fig. 4 shows the statistic results of the I_{cat} values in response to 1 mM ATCl and the Inhibit% of 22.6 μM DDVP to the I_{cat} values, at various fabrication conditions. Firstly, the CS content in the TiO_2-CS nanocomposites was varied, when the TiO_2 sol-gel content was kept at 90.0% (Fig. 4A). The I_{cat} value shows a growing tendency with the increase of the CS content, and the DDVP Inhibit% has no obvious changes, at the CS content lower than ~0.005%. The enhanced ATCl response should be mainly due to an improved mechanical stability and an increased AChE immobilization amount resulting from the rougher nanostructure as probed by SEM. However, the CS incorporation with content higher than ~0.005% caused obvious decreases both for the I_{cat} values and for the DDVP Inhibit%. High CS content could also compromise the nanocomposite conductivity, and result in much coagulated nanogel, thus leading to low electrocatalytic activity, and slightly limiting the permeation of ATCl, TCl and OPs molecules through the immobilization matrix. The optimum CS content was thus decided as 0.005%. The content of the TiO_2 sol-gel precursor in the TiO_2-CS solution was then optimized. The I_{cat} value increased monotonically with the increase of the TiO_2 content from 90.0% to 99.0%, and then sharply dropped with further increase of the TiO_2 content (Fig. 4B). High TiO_2 sol-gel content would result in large immobilization matrix amount, thus large amount of immobilized AChE. However, when the TiO_2 sol-gel content is too high, the homogeneity of the nanocomposite could not be realized. The optimum TiO_2 sol-gel precursor content was therefore chosen as 99.0%. Afterwards, the electrodeposition time for forming the CS layer was optimized to be 20 s, as the I_{cat} value was the highest at the time of 15 ~ 20 s (Fig. 4C). As discussed before, the CS layer is a very important component in the as-fabricated biosensor by serving as a positively charged interface to effectively adsorb and immobilize the negatively charged AChE. However, introduction of the CS layer would also decrease the conductivity of the biosensor, and limit more or less the permeation of TCl through the matrix. In contrast, the DDVP Inhibit% was not obviously affected by the CS layer thickness (Inset in Fig. 4C), suggesting that the CS layer does not affect the OPs molecules in contacting with the immobilized AChE. This was expected as much portion of the AChE molecules should be adsorbed on the outer surface of the CS layer (as shown in Scheme 1). Finally, the AChE loading concentration was optimized as 5 mg mL^{-1}, a saturation concentration for AChE immobilization (Fig. S-5 in Supplementary Material).

3.4. Electrocatalytic activity and analytical performance

At the optimum fabrication conditions, the electrocatalytic activity was investigated by recording the DPV curves in various concentrations of ATCl (Fig. 5A). The signal increased monotonically with the increase of ATCl concentration from 0.1 to 9 mM, and follows the Michaelis–Menten kinetics. A linear $1/I_{cat}$ (μA^{-1}) vs. $1/C_{ATCl}$ (mM^{-1}) plot (Inset in Fig. 5A) was obtained with a regression equation of $1/I_{cat} = 0.22 + 0.68 \times 1/C_{ATCl}$ (R = 0.9773 = 0.9773). By using the Lineweaver-Burk equation (Eq. (2)), the apparent Michaelis–Menten constant (K_m) was obtained to be 3.1 mM.

$$\frac{1}{I_{cat}} = \frac{K_m}{I_{max}} \times \frac{1}{C_{ATCl}} + \frac{1}{I_{max}} \quad (2)$$

The analytical performance of the enzyme biosensor to DDVP was then evaluated. Fig. 5B illustrates the DPV curves of the biosensor in 1 mM ATCl before (curve a) and after (curve b) incubation with 22.6 μM DDVP. The I_{cat} value decreased dramatically from 1.66 μA to 0.34 μA, due to the DDVP inhibition. The plot of Inhibit% versus the DDVP concentration (C_{DDVP}) (Inset in Fig. 5B) shows two linear

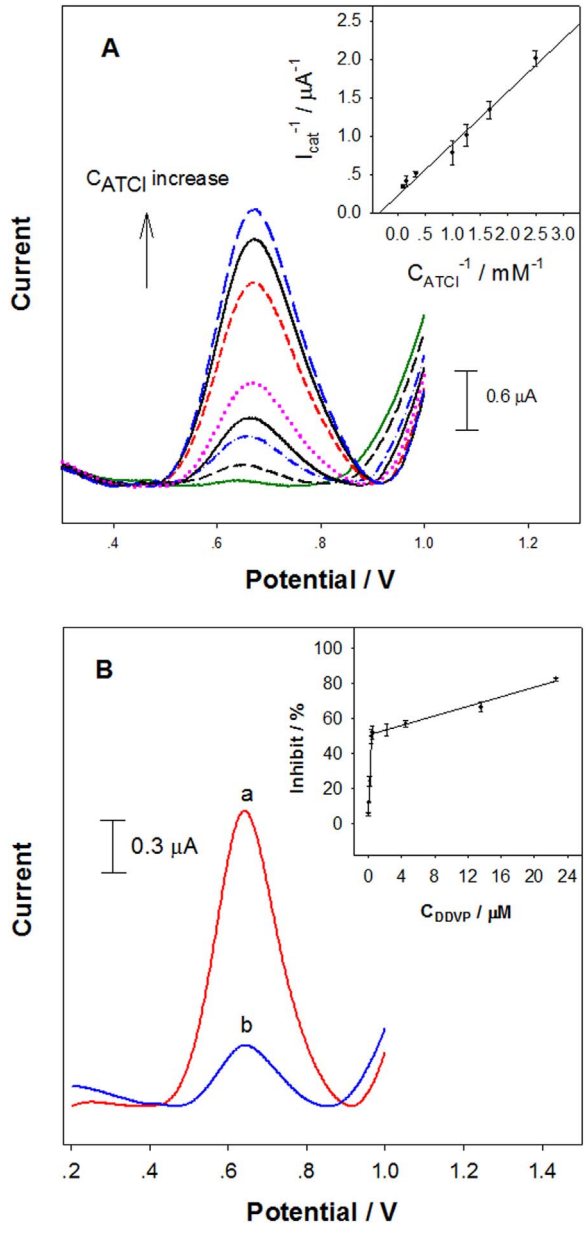

Fig. 5. (A) The DPV responses of the AChE/CS@TiO_2^m-CS^m/rGO/GC electrode to various concentrations of ATCl. Inset: the plot of $1/I_{cat}$ versus $1/C_{ATCl}$. n = 3. (B) The DPVs of the AChE/CS@TiO_2^m-CS^m/rGO/GC electrode in 1 mM ATCl, (a) before and (b) after incubated in 22.6 μM DDVP. Inset: the Inhibit% values by various concentrations of DDVP. The electrodeposition time for CS layer: 20 s, AChE concentration: 5 mg mL^{-1}. n = 3–7.

ranges: from 0.036 μM (7.9 ppb) to 0.453 μM; and from 0.453 μM to 22.6 μM, with the regression equation of Inhibit% = −0.01 + 137.21 × C_{DDVP}; and Inhibit% = 50.61 + 1.35 × C_{DDVP}, and a regression coefficient of 0.9998 and 0.9966, respectively. The limit of detection (LOD) was 29 nM (6.4 ppb) (calculated in a 3σ rule). The biosensor is very reproducible. The Inhibit% for 22.6 μM DDVP with 7 different biosensor preparations was 81.60% ± 1.18% (mean ± S.D.), with an RSD value of only 1.44%. The performance of the biosensor is compared with those of other reported electrochemical AChE biosensors (Table S-1 in Supplementary Material). The LOD value of the biosensor is comparable or superior to some of the reported values, and the linear range is broader than most of the reported values. In addition, it should be noted that for our biosensor, the lowest value (7.9 ppb) in the linear range is superior than most of the reported values, and both the LOD value and the lowest value in the linear range are lower than the maximum residue limits (MRLs) for DDVP (10 ppb) as reported in the European Union pesticides database as well as those from the U.S. Department Agriculture. Most importantly, the stability of our biosensor, which is a very important character for its practical applicability, is very excellent. The responses to 1 mM ATCl are very repetitive, exhibiting an RSD value of only 1.49% for 4 detections. During both the dry and wet storages, the signal intensity has no any diminishment during the tested storage period of 30 days. The very excellent stability should attribute to both the incorporation and electrodeposition of CS into/on the TiO_2 immobilization matrix, which strengthen the TiO_2 film and reinforce the AChE immobilization through an electrostatic interaction.

Finally, the applicability of the biosensor was evaluated (Table S-2). For the DDVP added in the cabbage juice samples, the recovery ratios were all within the range of 100 ± 3%, the RSDs were less than 10.0%, indicating a very accurate OPs detection with the biosensor.

4. Conclusions

A multi-layered immobilization matrix was prepared simply by layer-by-layer casting and electrodeposition, and AChE was immobilized through adsorption. The matrix has a mesoporous nanostructure, which not only provides a biocompatible microenvironment and a large surface area for AChE loading, and also facilitates the electrocatalytic oxidation of TCl. Both the CS layer and the incorporated CS drastically improved the mechanically stability of the nanocomposites. In addition, the positively charged CS layer reinforces an effective AChE immobilization. The developed AChE biosensor shows high stability, reproducibility, sensitivity, and accuracy in detection DDVP, the model OPs compound, provided to be an efficient platform for immobilization of AChE, and a promisingly applicable OPs biosensor with high reliability, simplicity, and rapidness.

Acknowledgments

This work was financially supported by Plan for Scientific Innovation Talent of Henan Province to H.F. Cui, the National Natural Science Foundation of China (NSFC 21345007), and the Henan Open-up and Collaboration Program of Science and Technology (132106000070).

Appendix A. Supplementary material

Supplementary data associated with this article can be found in the online version at doi:10.1016/j.bios.2017.07.068.

References

Bai, Y.F., Zhang, Y.F., Zhou, A.W., Li, H.W., Zhang, Y., Luong, J.H., Cui, H.F., 2014b. Nanotechnology 25, 405601.
Balandin, A.A., Ghosh, S., Bao, W., Calizo, I., Teweldebrhan, D., Miao, F., Lau, C.N., 2008. Nano Lett. 8, 902–907.
Behera, S.S., Das, U., Kumar, A., Bissoyi, A., Singh, A.K., 2017. Int. J. Biol. Macroml. 98, 329–340.
Chen, M., Hou, C., Huo, D., Dong, L., Yang, M., Fa, H., 2016. Nano 11, 1650128.
Choi, J.W., Kim, Y.K., Lee, I.H., Min, J., Lee, W.H., 2001. Biosens. Bioelectron. 16, 937–943.
Costa, L.G., 2006. Clin. Chim. Acta 366, 1–13.
Cui, H.F., Zhang, K., Zhang, Y.F., Sun, Y.L., Wang, J., Zhang, W.D., Luong, J.H., 2013. Biosens. Bioelectron. 46, 113–118.
Dvir, H., Silman, I., Harel, M., Rosenberry, T.L., Sussman, J.L., 2010. Chem.-Biol. Interact. 187, 10–22.
Eddleston, M., Buckley, N.A., Eyer, P., Dawson, A.H., 2008. Lancet 371, 597–607.
Feng, H.B., Cheng, R., Zhao, X., Duan, X.F., Li, J.H., 2013. Nat. Commun. 4, 1539.
Fukuto, T.R., 1990. Environ. Health Persp. 87, 245–254.
Gao, H., Luo, G., Feng, J., Ottova, A.L., Tien, H.T., 2001. J. Electroanal. Chem. 496, 158–161.
Ge, S.G., Lan, F.F., Lang, L.L., Ren, N., Li, L., Liu, H.Y., Yan, M., Yu, J.H., 2017a. ACS Appl. Mater. 9, 6670–6678.
Ge, S.G., Zhang, L.N., Zhang, Y., Lan, F.F., Yan, M., Yu, J.H., 2017b. Nanoscale 9, 4366–4382.

Geim, A.K., 2009. Science 324, 1530–1534.
Li, Y., Shi, L., Han, G., Xiao, Y., Zhou, W., 2017. Sens. Actuat B-Chem. 238, 945–953.
Long, Q., Li, H., Zhang, Y., Yao, S., 2015. Biosens. Bioelectron. 68, 168–174.
Lu, L., Xia, Y., 2015. Anal. Chem. 87, 8584–8591.
Novoselov, K.S., Geim, A.K., Morozov, S.V., Jiang, D., Zhang, Y., Dubonos, S.V., Grigorieva, I.V., Firsov, A.A., 2004. Science 306, 666–669.
Park, S., Ruoff, R.S., 2009. Nat. Nanotech. 4, 217–224.
Patocka, J., Kuca, K., Jun, D., 2004. Acta Med. 47, 215–228.
Qian, S., Lin, H., 2015. Anal. Chem. 87, 5395–5400.
Ripoll, D.R., Faerman, C.H., Axelsen, P.H., Silman, I., Sussman, J.L., 1993. Proc. Natl. Acad. Sci. USA 90, 5128–5132.
Shi, M., Xu, J., Zhang, S., Liu, B., Kong, J., 2006. Talanta 68, 1089–1095.
Sundarmurugasan, R., Gumpu, M.B., Ramachandra, B.L., Nesakumar, N., Sethuraman, S., Krishnan, U.M., Rayappan, J.B.B., 2016. Sens. Actuat B-Chem. 230, 306–313.
Tang, L., Wang, Y., Liu, Y., Li, J., 2011. Acs Nano 5, 3817–3822.
Tang, Y., Hu, X., Zhang, X., Guo, D., Zhang, J., Kong, F., 2016. Carbohyd. Polym. 151, 752–759.
Wang, H., Zhao, G., Chen, D., Wang, Z., Liu, G., 2016. Int. J. Electrochem. Sci. 11, 10906–10918.
Wei, M., Wang, J., 2015. Sens. Actuat B-Chem. 211, 290–296.
Yang, G., Su, J., Guo, Y., Xu, H., Ke, Q., 2017. J. Mater. Sci. 52, 5404–5416.
Yu, G., Wu, W., Zhao, Q., Wei, X., Lu, Q., 2015. Biosens. Bioelectron. 68, 288–294.
Yu, J., Ju, H., 2002. Anal. Chem. 74, 3579–3583.
Zhu, Y., Cao, H., Tang, L., Yang, X., Li, C., 2009. Electrochim. Acta 54, 2823–2827.